Demonstration of record-low injection-current variable optical attenuator based on strained SiGe with optimized lateral *pin* junction

Younghyun Kim,[1*] Junichi Fujikata,[2] Shigeki Takahashi,[2] Mitsuru Takenaka, [1] and Shinichi Takagi[1]

[1]*Dept. of Electrical Engineering and Information Systems, The University of Tokyo 7-3-1 Hongo, Bunkyo-ku, Tokyo 113-0032, Japan*

[2]*Photonics Electronics Technology Research Association (PETRA), 16-1, Onogawa, Tsukuba 305-8569, Japan*

**yhkim@mosfet.t.u-tokyo.ac.jp*

Abstract: We demonstrate a strained SiGe variable optical attenuator (VOA) with a lateral *pin* junction which exhibits record-low injection-current for 20-dB attenuation. We optimize the distance between the highly doped p + and n + regions in the lateral *pin* junction to effectively inject electrons and holes, taking into account the propagation loss. In conjunction with the enhanced free-carrier absorption in strained SiGe, the SiGe VOA with the optimized lateral *pin* junction exhibits 20-dB attenuation by 20-mA/mm injection current, which is 1.5 times lower current density than that of the Si VOA. The SiGe VOA also shows better RF response than the Si VOA due to the short carrier lifetime in SiGe, allowing us to achieve efficient and fast attenuation modulation simultaneously. Furthermore, 2-GHz switching and error-free transmission of 4 × 12.5 Gbps WDM signal have been also achieved.

OCIS codes: (130.3120) Integrated optics devices; (250.7360) Waveguide modulators.

References and links

1. Y. A. Vlasov, "Silicon CMOS-Integrated Nano-Photonics for Computer and Data Communications Beyond 100GElectrooptical Effects in Silicon," IEEE Commun. Mag. **50**(2), S67–S72 (2012).
2. G. T. Reed, G. Mashanovich, F. Y. Gardes, and D. J. Thomson, "Silicon optical modulators," Nat. Photonics **4**(8), 518–526 (2010).
3. D. Liang and J. E. Bowers, "Recent progress in lasers on silicon," Nat. Photonics **4**(8), 511–517 (2010).
4. J. Michel, J. F. Liu, and L. C. Kimerling, "High-performance Ge-on-Si photodetectors," Nat. Photonics **4**(8), 527–534 (2010).
5. Y. Vlasov and S. McNab, "Losses in single-mode silicon-on-insulator strip waveguides and bends," Opt. Express **12**(8), 1622–1631 (2004).
6. T. Tsuchizawa, K. Yamada, H. Fukuda, T. Watanabe, J. Takahashi, M. Takahashi, T. Shoji, E. Tamechika, S. Itabashi, and H. Morita, "Microphotonics devices based on silicon microfabrication technology," IEEE J. Sel. Top. Quant. **11**(1), 232–240 (2005).
7. F. Van Laere, W. Bogaerts, P. Dumon, G. Roelkens, D. Van Thourhout, and R. Baets, "Focusing Polarization Diversity Grating Couplers in Silicon-on-Insulator," J. Lightwave Technol. **27**(5), 612–618 (2009).
8. D. W. Zheng, B. T. Smith, and M. Asghari, "Improved efficiency Si-photonic attenuator," Opt. Express **16**(21), 16754–16765 (2008).
9. D. W. Zheng, B. T. Smith, J. Dong, and M. Asghari, "On the effective carrier lifetime of a silicon p-i-n diode optical modulator," Semicond. Sci. Technol. **23**(6), 064006 (2008).
10. P. Dong, S. Liao, H. Liang, R. Shafiiha, D. Feng, G. Li, X. Zheng, A. V. Krishnamoorthy, and M. Asghari, "Submilliwatt, ultrafast and broadband electro-optic silicon switches," Opt. Express **18**(24), 25225–25231 (2010).
11. H. Nishi, T. Tsuchizawa, T. Watanabe, H. Shinojima, K. Yamada, and S. Itabashi, "Compact and Polarization-Independent Variable Optical Attenuator Based on a Silicon Wire Waveguide with a Carrier Injection Structure," Jpn. J. Appl. Phys. **49**(4), 04DG20 (2010).
12. S. Park, K. Yamada, T. Tsuchizawa, T. Watanabe, H. Shinojima, H. Nishi, R. Kou, and S. Itabashi, "Influence of carrier lifetime on performance of silicon p-i-n variable optical attenuators fabricated on submicrometer rib waveguides," Opt. Express **18**(11), 11282–11291 (2010).

#233367 - $15.00 USD Received 28 Jan 2015; revised 20 Mar 2015; accepted 23 Mar 2015; published 1 May 2015

13. T. Tsuchizawa, K. Yamada, T. Watanabe, S. Park, H. Nishi, R. Kou, H. Shinojima, and S. Itabashi, "Monolithic Integration of Silicon-, Germanium-, and Silica-Based Optical Devices for Telecommunications Applications," IEEE J. Sel. Top. Quant. **17**(3), 516–525 (2011).
14. Y. Kim, J. Han, M. Takenaka, and S. Takagi, "Low temperature Al_2O_3 surface passivation for carrier-injection SiGe optical modulator," Opt. Express **22**(7), 7458–7464 (2014).
15. R. A. Soref and B. R. Bennett, "Electrooptical Effects in Silicon," IEEE. J, Quantum Electron. **23**(1), 123–129 (1987).
16. M. Takenaka and S. Takagi, "Strain Engineering of Plasma Dispersion Effect for SiGe Optical Modulators," IEEE. J, Quantum Electron. **48**(1), 8–16 (2012).
17. Y. Kim, M. Takenaka, T. Osada, M. Hata, and S. Takagi, "Strain-induced enhancement of plasma dispersion effect and free-carrier absorption in SiGe optical modulators," Sci Rep **4**, 4683 (2014).
18. Q. Xu, S. Manipatruni, B. Schmidt, J. Shakya, and M. Lipson, "12.5 Gbit/s carrier-injection-based silicon micro-ring silicon modulators," Opt. Express **15**(2), 430–436 (2007).
19. G. R. Zhou, M. W. Geis, S. J. Spector, F. Gan, M. E. Grein, R. T. Schulein, J. S. Orcutt, J. U. Yoon, D. M. Lennon, T. M. Lyszczarz, E. P. Ippen, and F. X. Käertner, "Effect of carrier lifetime on forward-biased silicon Mach-Zehnder modulators," Opt. Express **16**(8), 5218–5226 (2008).
20. K. Hammani, M. A. Ettabib, A. Bogris, A. Kapsalis, D. Syvridis, M. Brun, P. Labeye, S. Nicoletti, D. J. Richardson, and P. Petropoulos, "Optical properties of silicon germanium waveguides at telecommunication wavelengths," Opt. Express **21**(14), 16690–16701 (2013).

1. Introduction

Since the strong demand of data centers is growing rapidly, an electronic-photonic integrated circuit (EPIC) is going to be a promising solution to provide broadband, low-power, and high-density optical interconnections for the data center network [1]. Among various platforms for EPICs, Si photonics is a key technology, by which photonic components including lasers, optical modulators, photodetectors, and passive waveguide devices have been dramatically developed in the past ten years [2–7]. Si-based variable optical attenuators (VOAs) are also necessary components for controlling optical power levels in EPICs. Si VOAs based on the free-carrier absorption have been mostly investigated and demonstrated using carrier injection through a forward-biased lateral *pin* junction [8–14]. However, the efficiency in absorption modulation is still low due to the small free-carrier absorption in Si [15], resulting in high injection current and large power consumption. Therefore, it is indispensable to enhance the free-carrier effect for achieving low-power VOAs with a low injection current. To obtain the enhancement in the free-carrier effect, we have proposed to use strained SiGe grown on Si, which is applicable to SiGe optical modulators, switches, and VOAs. The enhancement of the free-carrier effects, the plasma dispersion effect and the free-carrier absorption, is expected by reduction in the conductivity effective mass of holes in strained SiGe [15, 16]. Recently, we have demonstrated strain-induced enhancements in the plasma dispersion effect and free-carrier absorption for optical modulator and VOA applications by using the carrier-injection strained SiGe waveguide device with a lateral *pin* junction [17]. However, the first demonstration of the SiGe VOA in [17] was not fully optimized in terms of the distance between the heavily doped p + and n + regions, resulting in the low carrier injection efficiency. The diffusion length of injected carriers is limited various recombination processes. Therefore it is necessary to shorten the distance between the heavily doped regions as shown in Fig. 1.

In this paper, we demonstrate strained SiGe VOAs with high carrier injection efficiency through the optimization of the distance between the highly doped p + and n + regions by using electron beam (EB) lithography, taking into account the tradeoff between attenuator loss and carrier-injection efficiency. As a result, we have achieved the record-low injection current of 20 mA for 20-dB attenuation in the SiGe VOA. Furthermore, we have obtained 2-GHz switching and error-free transmission of 50-Gbps WDM signal.

#233367 - $15.00 USD Received 28 Jan 2015; revised 20 Mar 2015; accepted 23 Mar 2015; published 1 May 2015

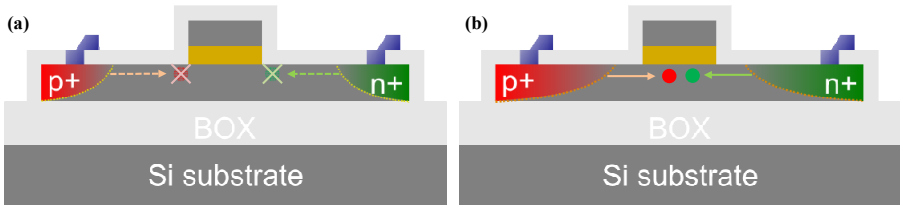

Fig. 1. Schematic of strained SiGe VOA with (a) long and (b) short lateral *pin* junction-distance.

2. Optimization of the distance between highly doped p + and n + regions

To effectively inject carriers into a waveguide core through a lateral pin junction, it is necessary to make the distance between highly doped p + and n + regions as short as possible due to the small diffusion length of carriers limited by recombination. However, the propagation loss caused by the free-carrier absorption in the highly-doped regions inevitably increases as the distance is reduced.

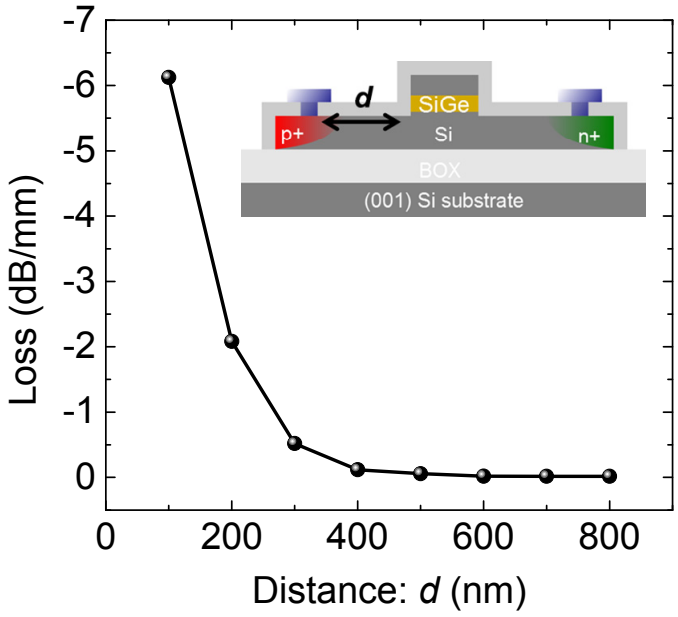

Fig. 2. Propagation loss as a function of the distance between the edge of the waveguide mesa and the highly-doped region.

First, we have investigated the propagation loss of the waveguide mode in terms of the distance between the edge of the waveguide mesa and the highly-doped region by the method of numerical analysis using by technology computer-aided design (TCAD) simulation and finite-difference optical mode analysis [16, 17]. The propagation loss is calculated by the overlap between the free-carrier distribution with 0 V bias and the fundamental transverse electric (TE) mode of the waveguide. Figure 2 shows the simulation result of propagation loss as a function of the distance between the edge of the waveguide mesa and the highly-doped region. When the distance is smaller than 400 nm, the propagation loss dramatically increases due to the free-carrier absorption in the heavily doped regions. As shown in Fig. 2, the propagation loss can be ignored when the distance is larger than 500 nm. In this study, we design the distance to be 650 nm, considering the process margin of EB lithography.

#233367 - $15.00 USD Received 28 Jan 2015; revised 20 Mar 2015; accepted 23 Mar 2015; published 1 May 2015

3. Device fabrication

We have fabricated strained SiGe VOAs using a (001) Si-on-insulator (SOI) wafer with a 250-nm-thick top Si layer and 2-μm-thick buried oxide (BOX) layer. To obtain the designed structure of Si/SiGe/SOI as shown in Fig. 3(a), we thinned the top Si layer down to 95 nm by thermal oxidation, then a 30-nm-thick fully strained $Si_{0.77}Ge_{0.23}$ layer and a 75-nm-thick Si layer were grown by chemical vapor deposition (CVD). The 600-nm-wide waveguide mesa was formed by EB lithography and dry etching as shown in Fig. 3(b). To form a lateral *pin* junction, we implemented the ion implantation of boron and phosphorus for the highly doped p + and n + regions, respectively, followed by the activation annealing in nitrogen atmosphere at 1000 °C. Due to the high thermal process, Ge diffusion occurs, which affect reduction in Ge fraction in the SiGe layer. After device fabrication, the Ge fraction is reduced to 14% [17]. Finally, the Al contact pads for the p + and n + regions were formed by thermal evaporation, followed by forming gas annealing at 400 °C to decrease contact resistances. Si VOAs are also fabricated at the same time.

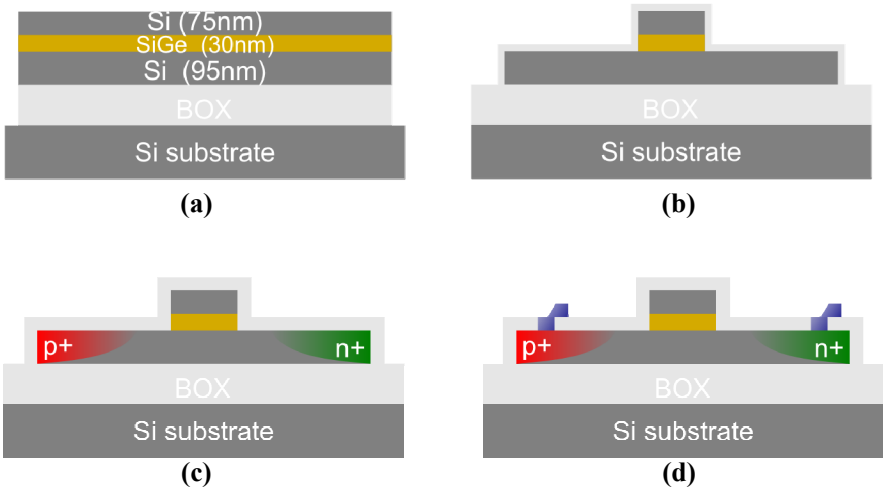

Fig. 3. Process flow of strained SiGe VOA with lateral *pin* junction. (a) Si and SiGe growth on SOI, (b) waveguide formation (c) *pin* junction formation by ion implantation, and (d) Al contact formation.

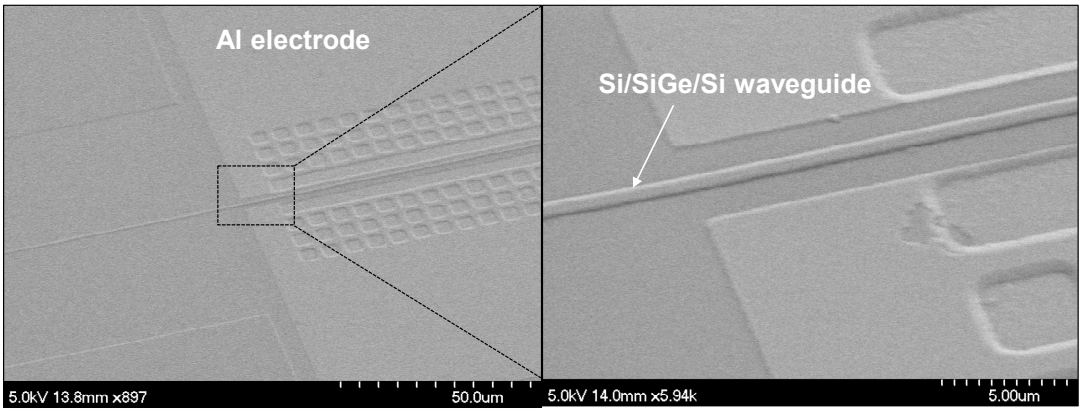

Fig. 4. SEM image of fabricated strained SiGe VOA.

#233367 - $15.00 USD Received 28 Jan 2015; revised 20 Mar 2015; accepted 23 Mar 2015; published 1 May 2015

We observed the fabricated SiGe device by scanning electron microscopy (SEM) as shown in Fig. 4. The tilted SEM image in Fig. 4 shows the well-defined Si/SiGe/Si waveguide and Al electrodes formed by EB lithography.

4. Static characteristics

We measured the optical attenuation by injecting current to evaluate the device performance of the SiGe VOAs, including Si VOAs as reference devices. Continuous-wave (CW) light, which was polarized to a TE-like mode by a polarization controller, was coupled to the waveguide through a lensed fiber, which was in the wavelength range from 1.34 to 1.64 μm. Then, the output power was monitored using an InGaAs photodetector while changing the injection current through the *pin* junction. For calibrating the total coupling loss of approximately −30 dB, the insertion loss without injection current was subtracted from the measured output power. In terms of the thermal effect in the attenuation, the free-carrier absorption theoretically increases linearly with an increase in temperature. However, the temperature change is not significant when the injection current is below 50 mA/mm. We have analyzed the thermal change in the Si phase-shifter as a function of power consumption by COMSOL. Even when the power consumption is as high as 40 mW, the change is less than 10 K, which may result in a few percent changes in the free-carrier absorption. Furthermore, we used the thermal controller maintaining the constant temperature of sample stage to make the thermal effect as small as possible. Thus, the thermal effect is not significant in our experiments.

Figure 5(a) shows the measured optical attenuation versus the injected current density of the 1-mm-long SiGe and Si VOAs at a wavelength of 1.55 μm. As increasing injection current by forward-bias voltage, the optical attenuation increases due to the free-carrier absorption. The higher attenuation is shown for the SiGe VOA than the Si VOA at the same current density due to the enhanced free-carrier absorption in strained SiGe [17]. By optimizing the lateral *pin* junction structure, the injection current for 20-dB attenuation in the Si device as well as the SiGe device is reduced. For the SiGe VOA, the injection current density is as low as 20 mA/mm for 20-dB attenuation. The benchmark of injection current for 20-dB attenuation as a function of the distance between the p + and n + regions in the lateral *pin* junction is shown in Fig. 5(b). It is notable that the current required for 20-dB attenuation decreases with decreasing the junction distance due to improved carrier injection efficiency. Therefore, the optical attenuation property is improved by shortening the distance between p + and n + regions. In the SiGe VOA, we achieved record-low injection current of 20 mA/mm for 20-dB attenuation thanks to the optimization and strain effect in SiGe [17] as compared with Si VOAs reported so far [12, 13].

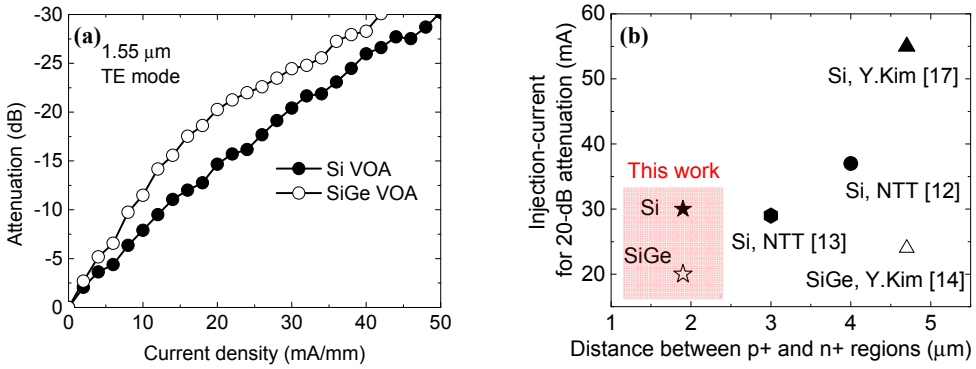

Fig. 5. (a) Attenuation characteristics as a function of current density for Si and SiGe VOAs and (b) benchmark of Si and SiGe VOAs.

We show the wavelength dependence of the SiGe VOA in Fig. 6. Figure 6(a) shows the transmission spectra of the SiGe VOA from 1.34 to 1.64 μm with 0 and 30 mA/mm injection

#233367 - $15.00 USD Received 28 Jan 2015; revised 20 Mar 2015; accepted 23 Mar 2015; published 1 May 2015

current. We achieved the wide optical bandwidth despite bandgap shrinkage in strained SiGe [16, 17]. Figure 6(b) shows the optical attenuation at injection currents of 5, 15, and 25 mA/mm as a function of the square of the wavelength. It is shown that the attenuation and the square of the wavelength have clear linear relationship, indicating the optical attenuation is from the free-carrier absorption.

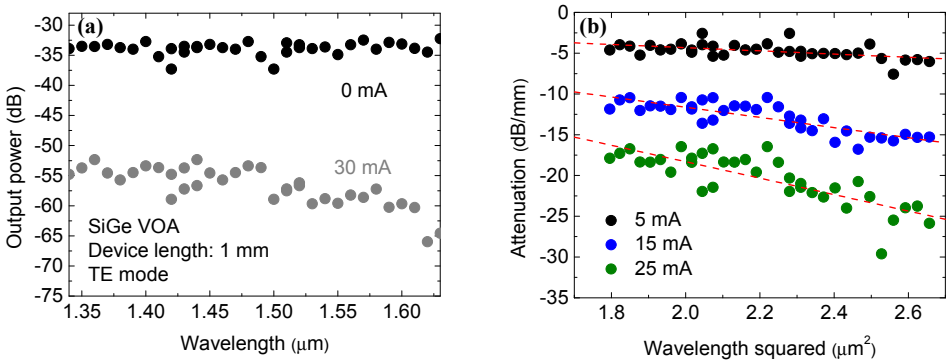

Fig. 6. Wavelength dependence of (a) transmission and (b) attenuation of SiGe VOA.

Figure 7 shows current density vs. voltage (I-V) characteristics of the lateral *pin* junctions in the SiGe and Si VOAs. It is found that the threshold voltage of the SiGe VOA is smaller than that of the Si VOA due to the reduction in built-in potential by strained SiGe. It is interesting to note that the reduction in the threshold voltage can contribute low-power operation especially for optical modulators and switches. In terms of the power consumption between the SiGe and Si VOAs, the SiGe and Si VOAs have approximately 22 mW and 36 mW for 20-dB attenuation, respectively. The power consumption of the SiGe device is reduced by an half of the reported value [17] due to the *pin* junction optimization for the distance.

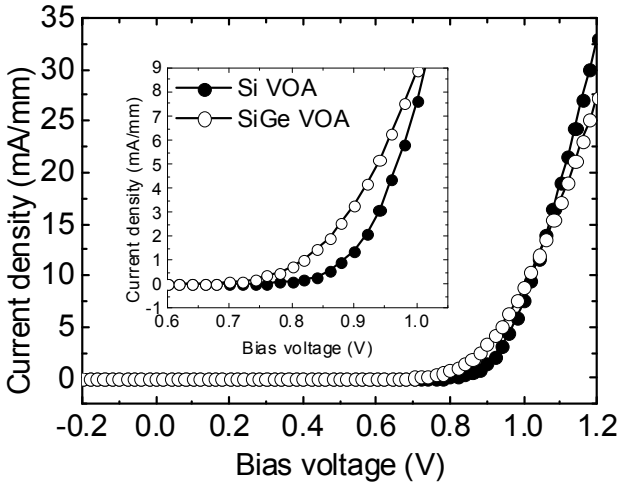

Fig. 7. I-V characteristics of *pin* junctions of Si and SiGe VOAs.

5. Dynamic characteristics

We carried out the RF measurement for the dynamic characteristics. We investigated the small-signal frequency response of Si and SiGe VOAs as shown in Fig. 8(a). Although the response is limited by the minority carrier lifetime in case of forward-biased *pin* junctions [12], the SiGe VOA shows the better frequency response than the Si VOA. The 3-dB

#233367 - $15.00 USD Received 28 Jan 2015; revised 20 Mar 2015; accepted 23 Mar 2015; published 1 May 2015

bandwidth in the SiGe VOA is approximately improved by 1.5 times. Also, we have obtained 2-GHz switching operation at a bias voltage of 0.77 V with the pre-emphasis method [18] as shown in Fig. 8(b).

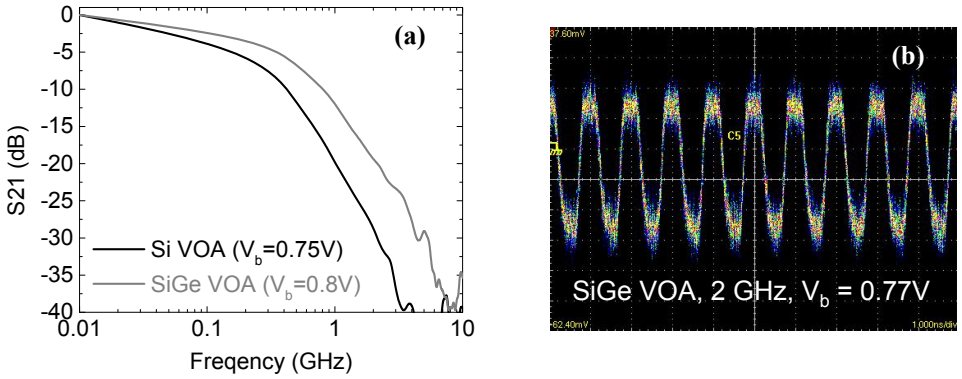

Fig. 8. (a) Frequency response and (b) sine-wave response at 2 GHz of SiGe VOA.

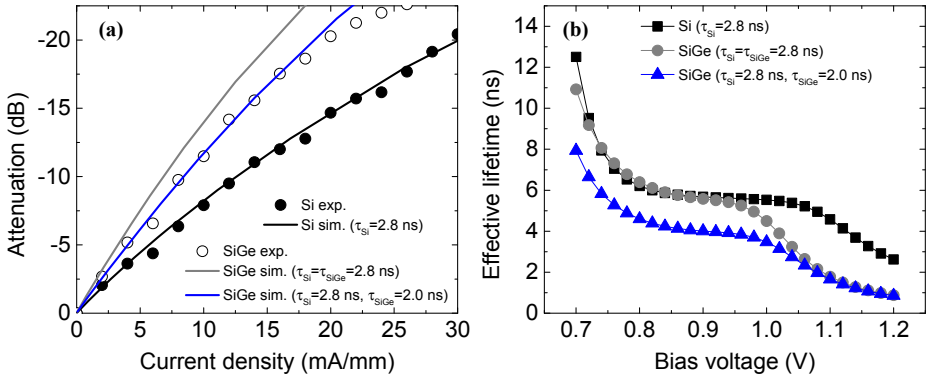

Fig. 9. (a) Experiment and simulation results of Attenuation in SiGe and Si VOAs as a function of current denstiy and (b) Effective lifetime for SiGe and Si VOAs.

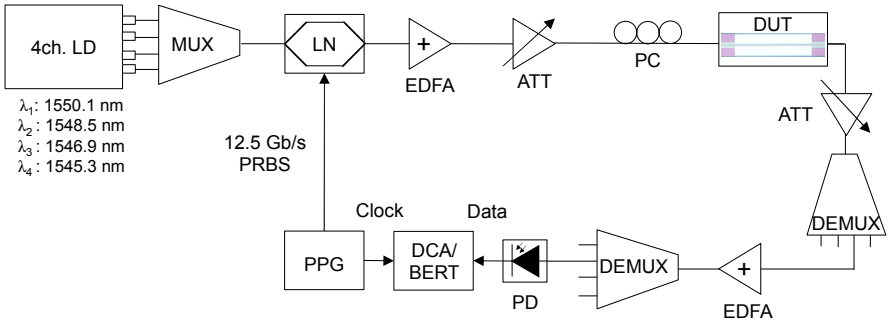

Fig. 10. Experimental setup for optical transmission test of 12.5 Gb/s PRBS signal.

The transmission characteristics for 50 Gb/s wavelength division multiplexing (WDM) signal were also evaluated under the measurement setup as shown in Fig. 10. 4 × 12.5 Gb/s non-return-to-zero (NRZ) 2^{31}-1 pseudo random bit sequence (PRBS) optical signals was fed into the SiGe VOA. The total input power was approximately 18 dBm. The output signal was demultiplexed and evaluated by a digital communication analyzer (DCA) and a bit-error tester (BERT). Figure 11 shows the bit error rate (BER) curves of all the wavelength

#233367 - $15.00 USD Received 28 Jan 2015; revised 20 Mar 2015; accepted 23 Mar 2015; published 1 May 2015

channels. Although Ch. 4 exhibits relatively large power penalty which might be attributable to the nonlinear crosstalk in SiGe [20], error-free transmission for all the channels with clear eye openings were successfully obtained.

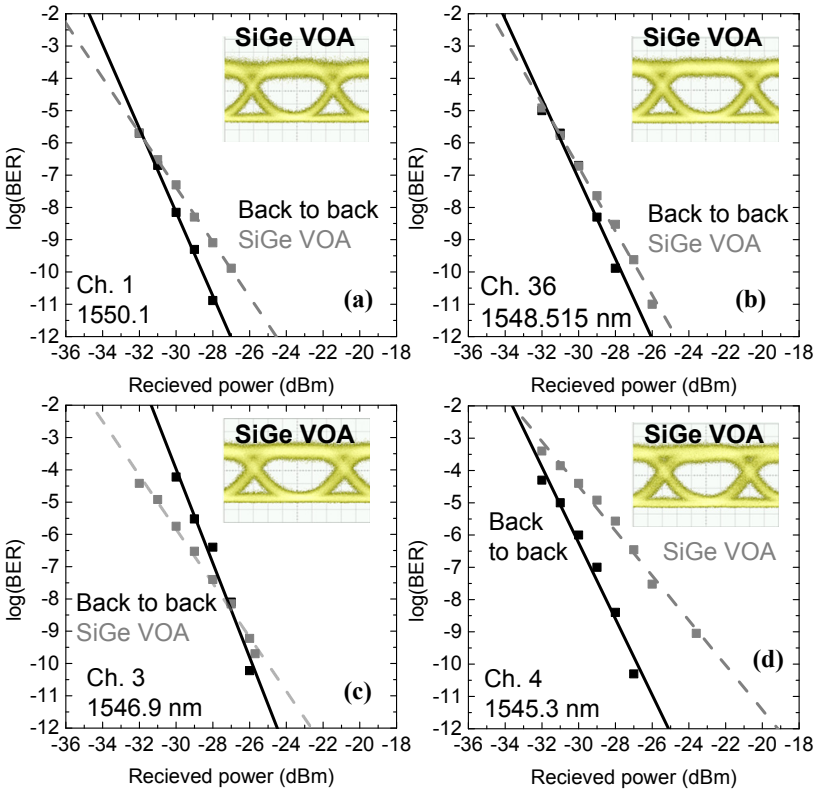

Fig. 11. BER after transmission of 4 × 12.5 Gb/s WDM signal through SiGe VOA.

6. Conclusion

We have demonstrated record-low injection-current SiGe VOAs by optimizing the distance between the p + and n + regions in the lateral *pin* junction. The injection current for 20-dB attenuation of the SiGe VOA is as low as 20 mA/mm thanks to the optimization and strain-induced enhancement of the free-carrier absorption in strained SiGe. We have also found 1.5 times improvement in the RF response of the SiGe VOA comparing to the Si VOA, and 2-GHz switching was achieved. Error-free transmission of 4 × 12.5 Gb/s WDM signal was also demonstrated.

Acknowledgments

This work was partly supported by the Strategic Information and Communications R&D Promotion Programme of the Ministry of Internal Affairs and Communications and NEDO in "Integrated Photonics-Electronics Convergence System Technology (PECST)". The authors would like to thank T. Osada and M. Hata, Sumitomo Chemical Company Ltd., Tsukuba, Japan, for their technical supports.

#233367 - $15.00 USD Received 28 Jan 2015; revised 20 Mar 2015; accepted 23 Mar 2015; published 1 May 2015